Kondo behavior and metamagnetic phase transition in the heavy-fermion compound $CeBi_2$

W. Zhou,[1] C. Q. Xu,[1] B. Li,[2] R. Sankar,[3] F. M. Zhang,[1] B. Qian,[1,*] C. Cao,[4] J. H. Dai,[4] Jianming Lu,[5] W. X. Jiang,[6] Dong Qian,[6] and Xiaofeng Xu[1,†]

[1]*Advanced Functional Materials Laboratory, Department of Physics, Changshu Institute of Technology, Changshu 215500, China*
[2]*Information Physics Research Center, Nanjing University of Posts and Telecommunications, Nanjing 210023, China*
[3]*Center for Condensed Matter Sciences, National Taiwan University, Taipei 10617, Taiwan*
[4]*Department of Physics, Hangzhou Normal University, Hangzhou 310036, China*
[5]*High Field Magnet Laboratory (HFML-EMFL), Radboud University, Toernooiveld 7, 6525ED Nijmegen, The Netherlands*
[6]*Key Laboratory of Artificial Structures and Quantum Control (Ministry of Education), School of Physics and Astronomy, Shanghai Jiao Tong University, Shanghai 200240, China*

(Received 21 February 2018; revised manuscript received 30 April 2018; published 11 May 2018)

Heavy fermions represent an archetypal example of strongly correlated electron systems which, due to entanglement among different interactions, often exhibit exotic and fascinating physics involving Kondo screening, magnetism, and unconventional superconductivity. Here we report a comprehensive study on the transport and thermodynamic properties of a cerium-based heavy-fermion compound $CeBi_2$ which undergoes an antiferromagnetic transition at $T_N \sim 3.3$ K. Its high-temperature paramagnetic state is characterized by an enhanced heat capacity with Sommerfeld coefficient γ over 200 mJ mol^{-1} K^{-2}. The magnetization in the magnetically ordered state features a metamagnetic transition. Remarkably, a large negative magnetoresistance associated with the magnetism was observed in a wide temperature and field-angle range. Collectively, $CeBi_2$ may serve as an intriguing system to study the interplay between the f electrons and the itinerant Fermi sea.

DOI: 10.1103/PhysRevB.97.195120

I. INTRODUCTION

The interactions between local moments and itinerant electrons may result in many exotic quantum phenomena, the heavy fermions in intermetallic lanthanide/actinide compounds being a clear-cut example [1]. In heavy fermions, the lattices of localized f moments are antiferromagnetically coupled with conduction electrons via Kondo interaction, and below a characteristic temperature, referred to as the Kondo coherence temperature, a Landau Fermi liquid with significantly enhanced electron effective mass emerges. Besides the Kondo interaction, the competing Ruderman-Kittel-Kasuya-Yosida interaction favors the magnetic ordering of the f moments [2,3].

Among heavy fermions, Ce-based compounds stand for the simplest example that incarnates most of the important physics since each Ce^{3+} ion has only one f electron in the $4f$ shell [4–8]. Specifically, many Ce-based antimonides/bismuthides display intriguing properties at low temperatures, including complex magnetic ordering, heavy-fermion behavior, unconventional superconductivity, or even nontrivial topological states [5,7,9,10]. Taking the rare-earth monoantimonide CeSb as an example, its magnetic resistivity logarithmically increases with decreasing T due to the incoherent Kondo scattering, and at least four metamagnetic transitions are observed in the magnetization curves [3,7]. More intriguingly, the angle-dependent magnetoresistance shows the signature of nontrivial Weyl fermions in its ferromagnetic state, which makes CeSb a promising candidate in the nascent search for novel topological states in the strongly correlated regime [7].

Another cerium-based intermetallic system, as yet much less studied, is cerium dibismuthide. A previous work focusing on the magnetization properties of $CeBi_2$ has reported the discovery of a metamagnetic phase transition [9]. However, similar to the Weyl semimetal candidate CeSb, the physical properties of the magnetic $CeBi_2$ deserve more fundamental exploration. In particular, it is not yet clear how universal the topological Weyl point seen in CeSb is in other Ce-based antimonides/bismuthides. In this context, we performed a systematic study on the transport and thermodynamic properties of $CeBi_2$ single crystals. Our study reveals that $CeBi_2$ is a typical Kondo lattice system with a large Sommerfeld coefficient γ over 200 mJ mol^{-1} K^{-2}. Contrasting with the topological origin of the negative magnetoresistance (MR) in CeSb [7], the negative MR in $CeBi_2$ can be instead associated with the complex magnetism of the system.

II. EXPERIMENT

Single crystals of $CeBi_2$ were grown by the self-flux method. Elemental Bi and Ce were mixed with a molar ratio over 10:1. The mixture was then sealed in a quartz tube in vacuum. The tube was heated to 1000 °C in a high-temperature box furnace and kept at this temperature for several hours. After a slow cooling process, platelike crystals which can be easily exfoliated were harvested.

Powder- and single-crystal x-ray diffraction (XRD) measurements were performed at room temperature using a Rigaku

*njqb@cslg.edu.cn
†xiaofeng.xu@cslg.edu.cn

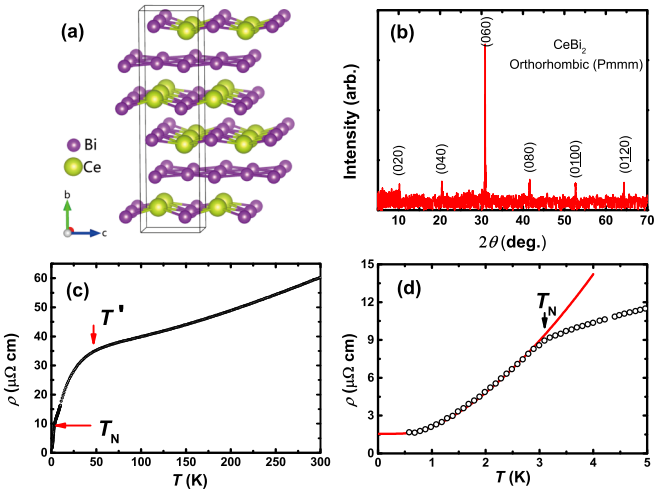

FIG. 1. (a) The crystal structure of $CeBi_2$. The single layers of Bi and the CeBi bilayers are alternately stacked along the b axis. The solid box indicates one conventional unit cell. (b) The x-ray-diffraction pattern for a $CeBi_2$ single crystal. (c) Temperature dependence of resistivity ρ of $CeBi_2$. T' and T_N denote two characteristic temperatures where ρ shows marked decreases with T. (d) A blowup of the low-T resistivity in panel (c). The red line is the fit to Eq. (1).

diffractometer with Cu $K\alpha$ radiation and a graphite monochromator. Low-field MR, angle-dependent MR, and specific-heat data were all collected on a Quantum Design (QD) physical property measurement system. The MR data in high magnetic field were acquired with a resistive Bitter magnet at the High Field Magnet Laboratory (HFML) (Nijmegen) with a maximum field of 35 T. The samples displayed highly symmetric resistance signals with respect to the magnetic-field direction, hence only data obtained for positive magnetic-field orientation are shown. The magnetization data were measured using a QD superconducting quantum interference device magnetometer with fields up to 7 T.

III. RESULTS

As shown in Fig. 1(a), the atomic structure of $CeBi_2$ is layered with single layers of Bi separated from each other by CeBi bilayers and stacked along the crystalline b axis. The Bi atoms in the Bi single layer are squarely coordinated, whereas in the CeBi bilayers, Ce atoms reside at the center of the square formed by four Bi atoms. A typical XRD pattern is shown in Fig. 1(b). Only the $(02\underline{\ell}0)$ peaks were observable, suggesting that the crystallographic b axis is perfectly perpendicular to the surface facet of the crystal. All $(02\underline{\ell}0)$ peaks can be well indexed with the orthorhombic ($Pmmm$, No. 47) space group, sharing the same structure as $LaBi_2$. Due to acute sensitivity to the air, the polycrystalline XRD patterns (data not shown) were only collected under the protection of Daphne 7373 oil. The resultant data show weak reflection, and as such the lattice parameters can only be roughly estimated to be $a = 4.71$, $b = 17.71$, $c = 4.57$ Å. Figure 1(c) depicts the T dependence of the electrical resistivity $\rho(T)$ for a $CeBi_2$ single crystal with current flowing along the ac plane. The resistivity of $CeBi_2$ is characterized by two sharp drops at temperatures T' and T_N. The resistivity drop at T' may be attributed either to the coherence in Kondo scattering or to the crystal electric-field (CEF) splitting of Ce atoms [11]. As will be seen below, the characteristic T_N can be assigned to an antiferromagnetic (AFM) phase transition. In the AFM state, the resistivity drops dramatically due to the reduction in electron-spin scattering in the ordered state. In the case of AFM systems with magnon dispersion of $\varepsilon_k = \sqrt{\Delta^2 + Dk^2}$, where Δ is the spin-wave gap which arises from anisotropy either in the magnetic interactions or of the single-ion type, and D is the spin-wave velocity, the resistivity takes the form [12–15],

$$\rho(T) = \rho_0 + A_\rho \Delta^2 \sqrt{\frac{T}{\Delta}} e^{-\Delta/T}\left[1 + \frac{2}{3}\left(\frac{T}{\Delta}\right) + \frac{2}{15}\left(\frac{T}{\Delta}\right)^2\right], \tag{1}$$

In this equation, the coefficient A_ρ is related to the spin-wave velocity by $A_\rho \propto D^{-3/2}$. As seen from Fig. 1(d), the resistivity of $CeBi_2$ in the AFM state fits well to the above formula, yielding $\rho_0 = 1.56\ \mu\Omega\,\mathrm{cm}$, $A_\rho = 1.25\ \mu\Omega\,\mathrm{cm}^{-1}\,\mathrm{K}^{-2}$, and $\Delta = 2.4$ K.

The specific heat of $CeBi_2$ is shown in Fig. 2(a). Under zero field, a sizable jump at T_N is observed, consistent with a second-order phase transition. Under a field of $H = 9$ T ($\| b$ axis), the jump is greatly suppressed, whereas the transition temperature shows no clear shift. At $T \sim 20$ K, the field has little effect on the heat capacity and two curves overlap [the upper inset of Fig. 2(a)]. The entropy under 9 T is approximately the same as that in 0 T at 20 K. The effect of the magnetic field on the

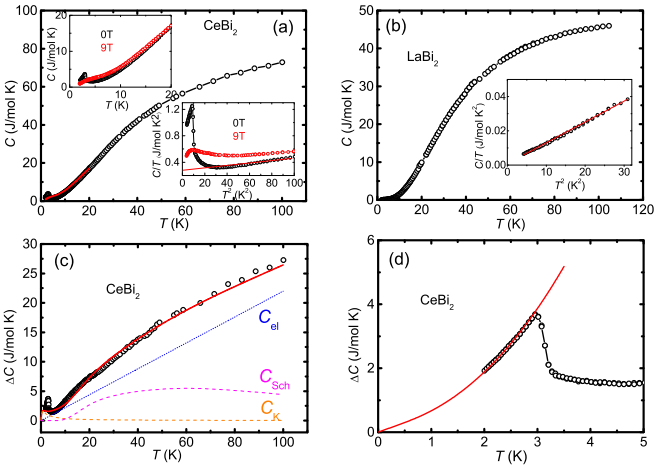

FIG. 2. (a) Temperature dependence of heat-capacity C of $CeBi_2$. The red line is the heat capacity under a 9-T field ($H \parallel b$). The upper inset shows the low-T heat capacity below 20 K. The lower inset manifests the data as C/T vs T^2 below 10 K. The red solid line is the linear extrapolation of the data. (b) Temperature dependence of the heat capacity of the reference compound $LaBi_2$. The inset is the low-T plot of C/T vs T^2 to separate the electronic and phononic contributions. (c) The nonphononic heat-capacity ΔC of $CeBi_2$. The thick red line is the fit to ΔC in the paramagnetic state, assuming the nonlattice contributions come from electron (C_{el}), Kondo (C_K), and CEF effect (C_{Sch}), each of which has also been plotted as individual lines. (d) Zoom in of the low-T ΔC in the AFM state. The red line is a fit to Eq. (2).

heat capacity is better seen when we plot $\frac{C}{T}$ as a function of T^2 [the lower inset of Fig. 2(a)]. In this manner, the electronic specific-heat coefficient γ can be estimated crudely as $\gamma \sim 200\ \mathrm{mJ\,mol^{-1}\,K^{-2}}$ if we linearly extrapolate the data from ~ 10 K (see the red solid line in the lower inset). The detailed analysis of heat capacity however will be given below.

To determine the electronic Sommerfeld coefficient γ of the sample, we refer to the specific heat of the nonmagnetic counterpart $LaBi_2$ crystal which is isostructural to $CeBi_2$. The phonon contribution to the heat capacity in $LaBi_2$ can be obtained by subtracting the electronic term which is determined by fitting the low-T heat capacity to $C(T) = \gamma T + \beta T^3$ as shown in the inset of Fig. 2(b). Assuming the same phononic heat capacity in $CeBi_2$ and $LaBi_2$, we can get the nonphononic heat-capacity ΔC of $CeBi_2$ as plotted in Fig. 2(c). In the paramagnetic region of a Kondo lattice, ΔC is composed of three components, i.e., $\Delta C = C_{\mathrm{el}} + C_K + C_{\mathrm{Sch}}$, where C_{el}, C_K, and C_{Sch} represent the electronic, Kondo, and Schottky terms, respectively [12]. The Kondo term C_K in a Kondo lattice is only dependent on the Kondo temperature T_K and was derived theoretically in the original papers by Schotte *et al.* [16,17]. The Schottky anomaly with energy gaps of Δ_1 and Δ_2, resulting from the Ce^{3+} crystal electric-field splitting, was considered [12]. Overall, these three terms can fit ΔC fairly well above T_N as demonstrated by the thick red line in Fig. 2(c), and the corresponding fitting parameters are $\gamma = 220\ \mathrm{mJ\,mol^{-1}\,K^{-2}}$, $\Delta_1 = 75$, $\Delta_2 = 190$, and $T_K = 1.5$ K. Their individual lines are also delineated in the figure. It is worth noting that the above fitting of the nonphononic heat capacity is based on the assumption of the same phonon

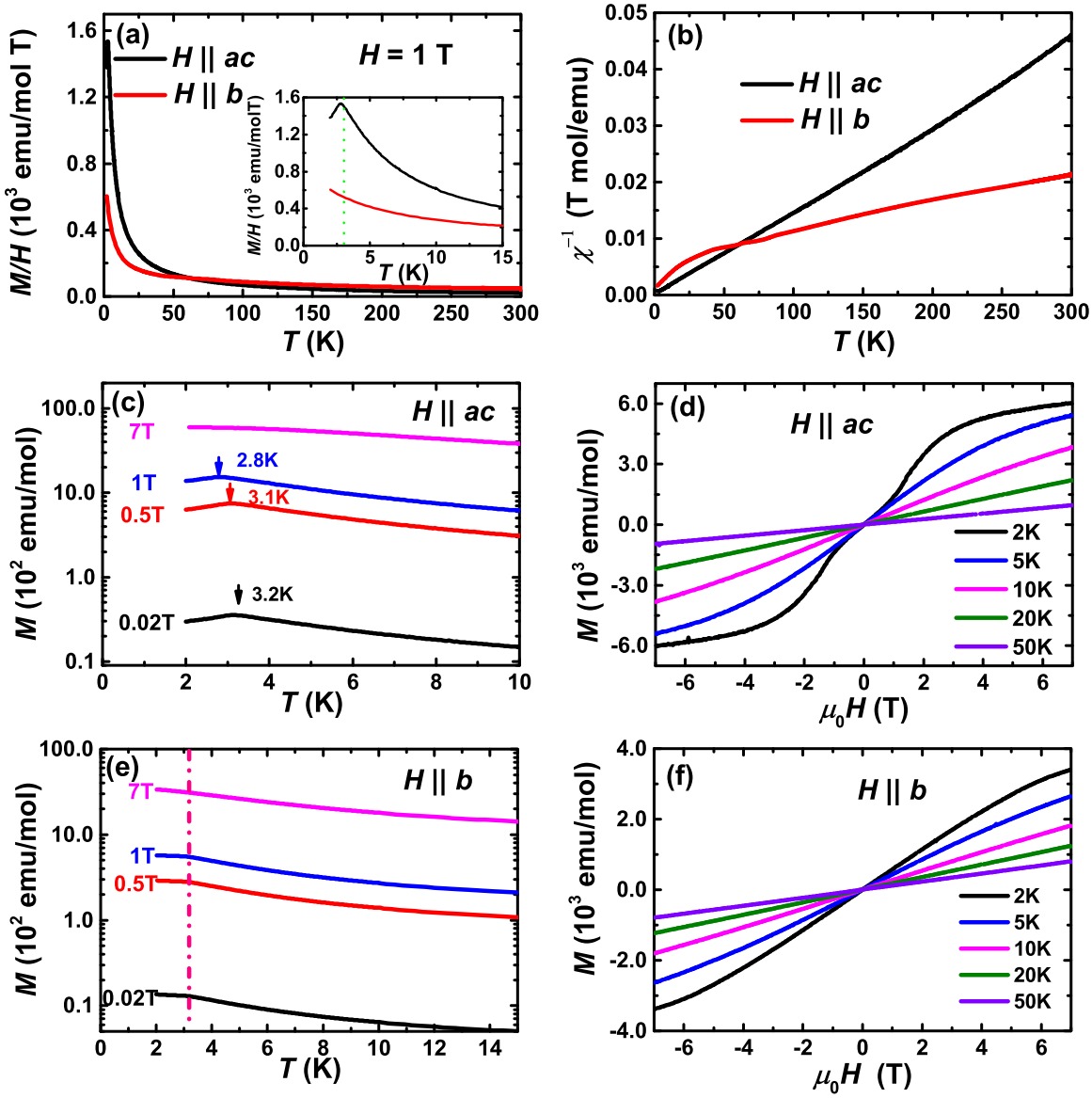

FIG. 3. (a) Temperature dependence of molar magnetic susceptibility of single-crystalline $CeBi_2$ measured under a field of 1 T oriented perpendicular and parallel to the b axis. (b) Inverse magnetic susceptibility as a function of temperature to demonstrate the Curie-Weiss law. (c) Magnetization under different fields ($H \parallel ac$). (d) Isothermal magnetization curves at some fixed temperatures for $H \parallel ac$. (e) Magnetization under different fields ($H \parallel b$). (f) Isothermal magnetization curves at some fixed temperatures for $H \parallel b$.

contribution in $CeBi_2$ and its counterpart $LaBi_2$. In the AFM state ($T < T_N$), in analogy to the above Eq. (1) for resistivity, ΔC has the form [14,18]

$$\Delta C = \gamma_m T + A_C \Delta^4 \sqrt{\frac{T}{\Delta}} e^{-\Delta/T} \times \left[1 + \frac{39}{20}\left(\frac{T}{\Delta}\right) + \frac{51}{32}\left(\frac{T}{\Delta}\right)^2\right], \quad (2)$$

where γ_m is the Sommerfeld coefficient in the magnetically ordered state and Δ is again the gap in the spin-wave spectrum [see Eq. (1)]. Although the fit range is limited, it gives $\Delta = 2.9$ K which is very close to the one obtained from the resistivity fit in Fig. 1(d). γ_m and A_C from the fit are 600 mJ mol^{-1} K^{-2} and 16 mJ mol^{-1} K^{-5}, respectively. Note that this γ_m is significantly enhanced compared with the one in the paramagnetic state, $\gamma \sim 220$ mJ mol^{-1} K^{-2}. Similar behaviors have been observed in other antiferromagnetic Kondo systems [12,13]. Different proposals other than what we used here to analyze the heat-capacity data in Kondo systems can also be found in the literature [19].

Figure 3 summarizes the magnetization measurements on $CeBi_2$ for both field orientations, i.e., the $H \parallel ac$ plane and $H \parallel b$ axis. Notable magnetization anisotropy is observed. As seen from the temperature dependence of the magnetic susceptibility (M/H) in Fig. 3(a), the susceptibility increases quickly below $\sim$50 K for both field directions. At $T \sim T_N$ (3.3 K), a pronounced peak in the M/H curve with $H \parallel ac$ is seen whereas for $H \parallel b$, only a weak inflexion point is observed as shown in the inset of Fig. 3(a), suggesting an antiferromagnetic phase transition. This anisotropic magnetization implies that the spins are aligned predominantly within the ac plane [20].

To further analyze the susceptibility, the data are plotted in panel (b) of Fig. 3 as χ^{-1} vs temperature to compare with the Curie-Weiss law. As seen, the Curie-Weiss law is roughly obeyed for $H \parallel ac$ whereas for $H \parallel b$, deviation is seen below

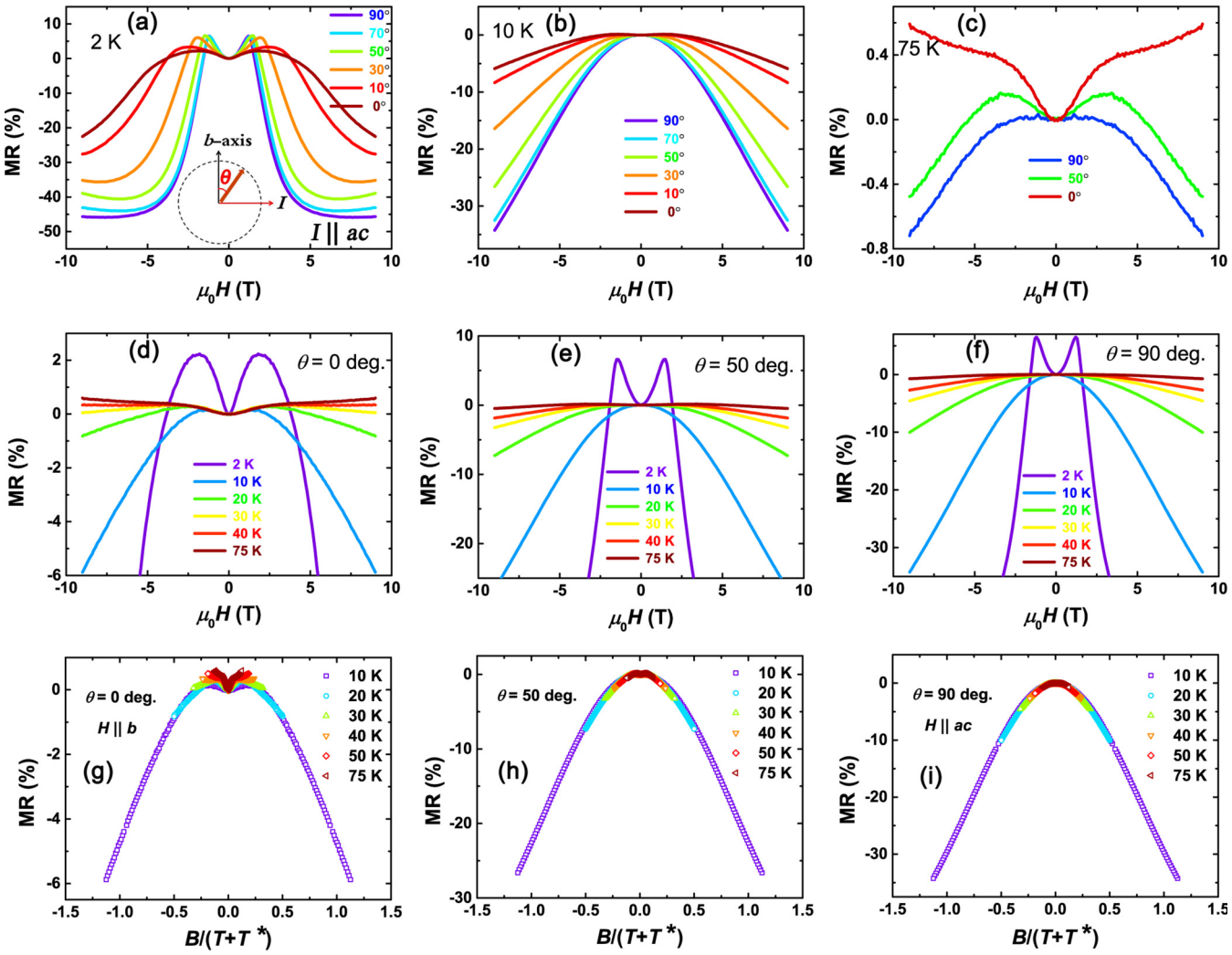

FIG. 4. (a)–(c) Field dependence of MR measured at various angles for three representative temperatures. The inset of panel (a) shows the field configurations. The current was set on the ac plane, and the field was confined on the plane constructed by the crystal b axis and the current flowing direction ($I \parallel ac$). θ is defined as the angle between the field direction and the crystal b axis. (d)–(f) MR measured at different temperatures for three representative angles. (g)–(i) The corresponding Schlottmann's scaling of the isothermal MR. T^* is the characteristic scaling temperature.

$\sim$50 K, presumably due to the CEF effects. We further extract the effective magnetic moment $\mu_{\rm eff}$ of Ce ions using the Curie-Weiss law: $\chi(T) = \frac{\mu_0 n \mu_{\rm eff}^2}{3k_B(T-\theta)}$, where n is the number of magnetic ions per mole and θ is a parameter related to the interaction between the ions. The fits give $\mu_{\rm eff} = 2.3\mu_B$, $\theta = -2$ K for $H \parallel ac$ and $\mu_{\rm eff} = 4.0\mu_B$, $\theta = -109$ K for $H \parallel b$. The value for $H \parallel ac$ is consistent with the theoretical value of $2.54\mu_B$ for a free Ce^{3+} ion whereas the latter is somewhat exaggerated.

Figure 3(c) shows the magnetization curves under different field strengths for $H \parallel ac$. As seen, the kink associated with the AFM transition is gradually suppressed to lower temperatures with increasing field and for $\mu_0 H > 2$ T, this kink disappears and a ferromagneticlike magnetization saturation at low temperatures emerges. This ferromagneticlike saturation is more notable on the isothermal magnetization curves in low-temperature regions [Fig. 3(d)]. Besides, when $T < T_N$, the $M(H)$ curves display a metamagnetic phase transition at field around 1.4 T, revealing a complex magnetic structure of $CeBi_2$. At 2 K and 7 T, the magnetization reaches a value of 6000 emu/mol that corresponds to the magnetic moment of $1.1\mu_B$, much lower than the saturated moment of the Ce^{3+} ion ($\mu_J \sim 2.14\mu_B$). Hence, more metamagnetic transitions are likely in higher fields. Each of the $M(H)$ curves was performed with both increasing and decreasing field strengths, yet no magnetic hysteresis was observed. By contrast, for $H \parallel b$, the magnetic properties become very different. First, the AFM transition temperature T_N shows no clear shift with increasing field strength [Fig. 3(e)]. Second, no obvious metamagnetic phase transition can be observed in the magnetization curves for $H \parallel b$ [Fig. 3(f)], indicating a rather strong magnetic anisotropy.

To explore the transport properties of $CeBi_2$, we performed the detailed magnetotransport measurements of $CeBi_2$ crystals at different temperatures and field angles. The field dependence of the MR, defined as $\mathrm{MR} = \frac{\rho(H)-\rho(0)}{\rho(0)} \times 100\%$, at different angles and for three representative temperatures is shown in Figs. 4(a)–4(c). The inset of Fig. 4(a) sketches the configuration of current flow (along the ac plane) and the field orientation. The magnetic field is constrained on the plane constructed by the crystal b axis and the current flow direction. Angle θ is defined as the angle between the field direction and the b axis. In the AFM ordered region [$T < T_N$, Fig. 4(a)], at $\theta = 90^\circ$, MR first increases rapidly with the field as expected for compounds in the AFM state. Beyond a certain field, MR decreases quickly, becomes negative, and finally saturates in the high fields. With the field rotated towards the b axis, both the positive and the negative MR effects are suppressed, and the evolution from the positive to negative MR with field becomes progressively smooth. With increasing temperature [Fig. 4(b)], qualitatively similar MR was seen, although the positive MR now becomes very weak. At $T = 75$ K, the MR becomes negligibly small, and only positive MR and an inflection point are seen for the $H \parallel b$ axis. Figures 4(d)–4(f) plot the MR at three angles under various temperatures. Similar behavior is seen for all these angles, although the size of the MR gets larger as the angle increases.

As is known, for a single-ion Kondo system, the MR curves measured under different temperatures can be scaled by Schlottmann's relation, where T^* is a scaling parameter related to magnetic correlation types [21]. Figures 4(f) and 4(g) show Schlottmann's scaling for three different angles for data measured above the AFM transition temperature T_N. As seen, for $H \parallel b$, Schlottmann's scaling is violated whereas for $H \parallel ac$ and for the intermediate angle ($\theta = 50^\circ$), all isothermal MR curves collapse onto a single curve, in good agreement with Schlottmann's theory. The best scaling yields a negative $T^* = -1.8$ K, implying the presence of ferromagnetic correlations in this antiferromagnetic system. Similar Schlottmann's scaling has also been observed in other heavy-fermion systems, such as $UBe_{1.3}$ [22], YbPtSn [23], and $CeNiGe_3$ [12,24]. The origin of the anisotropic violation of Schlottmann's scaling in $CeBi_2$ is unclear to us at present.

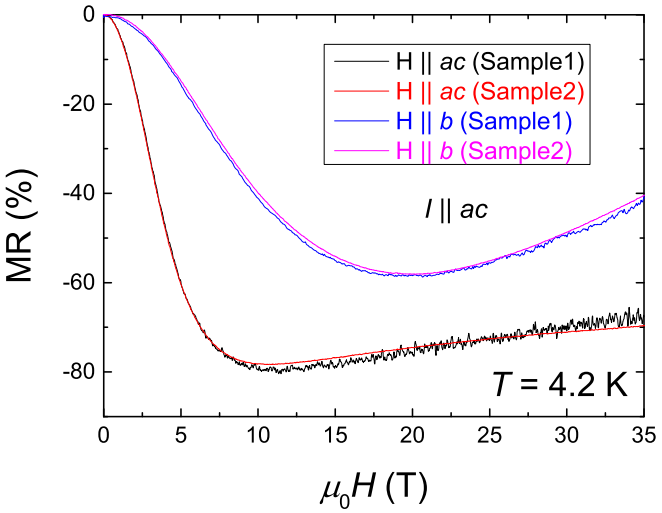

FIG. 5. MR at $T = 4.2$ K with fields up to 35 T for two single crystals (labeled as Sample 1 and Sample 2).

In Fig. 5, high-field MR measured up to 35 T for two pieces of samples at $T = 4.2$ K is shown. Note that these two samples show larger MR than that shown in Fig. 4 at the same field strengths due to higher sample purity. Although the MR behaviors are qualitatively similar to those shown in Fig. 4, the quasilinear MR in the high fields is intriguing and deserves more investigations in due course [25,26].

Finally, let us turn to consider the origin of the negative MR seen in this magnetic Kondo system. As shown in Fig. 6 [more pronounced in panel (b)], the initial field where the positive MR starts to change to the negative one coincides with the field for the metamagnetic phase transition, suggesting the possible symbiosis between these two phenomena. Besides, the MR saturates at the high field that may also be associated with the ferromagneticlike saturation seen in the magnetization curves. Therefore, it is reasonable to attribute the intriguing MR in this system to its intricate magnetism rather than the orbital effects or relativistic chiral anomaly physics [27,28].

IV. CONCLUSION

To summarize, we studied the detailed transport and thermodynamic properties of the antiferromagnetic Kondo system $CeBi_2$ that displays an antiferromagnetic transition with the Néel temperature T_N around 3.3 K. By analyzing the

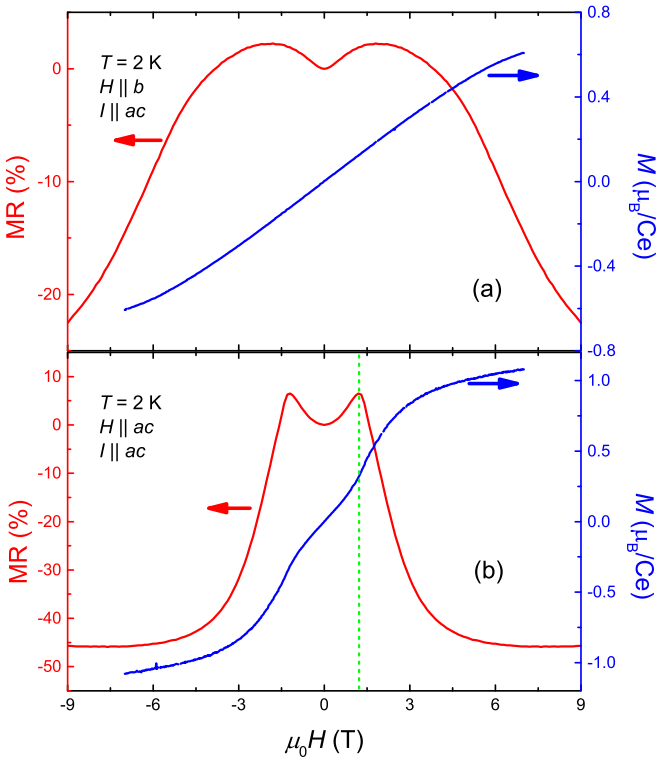

FIG. 6. Comparison between MR and magnetization for two field orientations at $T = 2$ K.

specific-heat data, we found the Sommerfeld coefficient γ over 200 mJ mol^{-1} K^{-2} in its paramagnetic state and a Kondo temperature of an order of $\sim$2 K. We presented the evidence that the large negative magnetoresistance observed in the wide temperature and field-angle ranges in this system is associated with its complex magnetism. $CeBi_2$ therefore represents an interesting system to formulate the theoretical understanding of the exotic consequences from the interplay between local f moments and itinerant conduction electrons.

ACKNOWLEDGMENTS

The authors would like to thank N. Hussey, X. Lu, Z. Mao, P. Biswas, and C. M. J. Andrew for the fruitful discussion. This work was sponsored by the National Key Basic Research Program of China (Grant No. 2014CB648400), by the National Natural Science Foundation of China (Grants No. 11474080, No. U1732162, No. U1632272, No. 11704047, and No. 11374043), by the Natural Science Foundation of Jiangsu Educational Department (Grant No. 15KJA430001), and six-talent peak of Jiangsu Province (Grant No. 2012-XCL-036). We acknowledge the support of the HFML, member of the European Magnetic Field Laboratory (EMFL). X.X. would also like to acknowledge financial support from an open program from Wuhan National High Magnetic Field Center (Grant No. 2015KF15).

W.Z. and C.Q.X. contributed equally to this work.

[1] G. R. Stewart, Heavy-fermion Systems, Rev. Mod. Phys. **56**, 755 (1984).

[2] Z. F. Weng, M. Smidman, L. Jiao, X. Lu, and H. Q. Yuan, Multiple quantum phase transitions and superconductivity in ce-based heavy fermions, Rep. Prog. Phys. **79**, 094503 (2016).

[3] S. Jang, R. Kealhofer, C. John, S. Doyle, J. Hong, J. H. Shim, Q. Si, O. Erten, J. D. Denlinger, J. G. Analytis, Direct visualization of coexisting channels of interaction in cesb, arXiv:1712.05817.

[4] S. L. Budko, P. C. Canfield, C. H. Mielke, and A. H. Lacerda, Anisotropic magnetic properties of light rare-earth diantimonides, Phys. Rev. B **57**, 13624 (1998).

[5] C. Petrovic, P. G. Pagliuso, M. F. Hundley, R. Movshovich, J. L. Sarrao, J. D. Thompson, Z. Fisk, and P. Monthoux, Heavy-fermion superconductivity in $CeCoIn_5$ at 2.3 K, J. Phys.: Condens. Matter **13**, 337 (2001).

[6] E. Bauer, G. Hilscher, H. Michor, C. Paul, E. Scheidt, A. Gribanov, Y. Seropegin, H. Noël, M. Sigrist, and P. Rogl, Heavy Fermion Superconductivity and Magnetic Order in Noncentrosymmetric $CePt_3Si$, Phys. Rev. Lett. **92**, 027003 (2004).

[7] C. Guo, C. Cao, M. Smidman, F. Wu, Y. Zhang, F. Steglich, F.-C. Zhang, and H. Yuan, Possible Weyl Fermions in the magnetic kondo system CeSb, npj Quantum Materials **2**, 39 (2017).

[8] L. Wang, Z. Fu, J. Sun, M. Liu, W. Yi, C. Yi, Y. Luo, Y. Dai, G. Liu, Y. Matsushita, K. Yamaura, L. Lu, J.-G. Cheng, Y.-F. Yang, Y. Shi, and J. Luo, Heavy fermion behavior in the quasi-one-dimensional kondo lattice $CeCo_2Ga_8$, npj Quantum Materials **2**, 36 (2017).

[9] C. Petrovic, S. Bud'ko, and P. C. Canfield, Anisotropic properties of rare-earth dibismites, J. Magn. Magn. Mater. **247**, 270 (2002).

[10] F. F. Tafti, Q. D. Gibson, S. K. Kushwaha, N. Haldolaarachchige, and R. J. Cava, Resistivity plateau and extreme magnetoresistance in LaSb, Nat. Phys. **12**, 272 (2015).

[11] R. A. Robinson, M. Kohgi, T. Osakabe, F. Trouw, J. W. Lynn, P. C. Canfield, J. D. Thompson, Z. Fisk, and W. P. Beyermann, Low-Energy Excitations and the Electronic Specific Heat of YbBiPt, Phys. Rev. Lett. **75**, 1194 (1995).

[12] A. P. Pikul, D. Kaczorowski, T. Plackowski, A. Czopnik, H. Michor, E. Bauer, G. Hilscher, P. Rogl, and Y. Grin, Kondo behavior in antiferromagnetic $CeNiGe_3$, Phys. Rev. B **67**, 224417 (2003).

[13] M. Szlawska and D. Kaczorowski,Magnetic ordering and kondo behavior in single-crystalline Ce_2NiSi_3, Phys. Rev. B **85**, 134423 (2012).

[14] M. B. Fontes, J. C. Trochez, B. Giordanengo, S. L. Budko, D. R. Sanchez, E. M. Baggio-Saitovitch, and M. A. Continentino, Electron-magnon interaction in RNiBC(R=Er, Ho, Dy, Tb, and Gd) series of compounds based on magnetoresistance measurements, Phys. Rev. B **60**, 6781 (1999).

[15] S. N. de Medeiros, M. A. Continentino, M. T. D. Orlando, M. B. Fontes, E. M. Baggio-Saitovitch, A. Rosch, and A. Eichler, Quantum critical point in $CeCo(Ge_{1-x}Si_x)_3$: Oral presentation, Phys. B **281**, 340 (2000).

[16] K. D. Schotte and U. Schotte, Intepretation of Kondo experiments in a magnetic field, Phys. Lett. A **55**, 38 (1975).

[17] U. Desgranges and K. D. Schotte, Specific heat of the kondo model, Phys. Lett. A **91**, 240 (1982).

[18] M. A. Continentino, S. N. de Medeiros, M. T. D. Orlando, M. B. Fontes, and E. M. Baggio-Saitovitch, Anisotropic quantum critical behavior in $CeCoGe_{3-x}Si_x$, Phys. Rev. B **64**, 012404 (2001).

[19] V. T. Rajan, Magnetic Susceptibility and Specific Heat of the Coqblin-Schrieffer Model, Phys. Rev. Lett. **51**, 308 (1983).

[20] X. Xu, A. Carrington, A. I. Coldea, A. Enayati-Rad, A. Narduzzo, S. Horii, and N. E. Hussey, Dimensionality-driven spin-flop transition in quasi-one-dimensional $PrBa_2Cu_4O_8$, Phys. Rev. B **81**, 224435 (2010).

[21] P. Schlottmann, Some exact results for dilute mixed-valent and heavy-fermion systems, Phys. Rep. **181**, 1 (1989).

[22] B. Andraka and G. R. Stewart, Scaling in the magnetoresistance of single-crystalline UBe_{13}, Phys. Rev. B **49**, 12359 (1994).

[23] R. Pietri, B. Andraka, D. Kaczorowski, A. Leithe-Jasper, and P. Rogl, Magnetoresistance and low-temperature specific heat of the Yb compounds YbRhSn, YbPdBi, and YbPtSn, Phys. Rev. B **61**, 12169 (2000).

[24] H. Sato, Y. Aoki, J. Urakawa, H. Sugawara, Y. Onuki, T. Fukuhara, and K. Maezawa, Hall effect in $Y_{1-x}U_xPd_3$ and $CeNi_2Ge_2$, Phys. Rev. B **58**, R2933(R) (1998).

[25] C. Q. Xu, W. Zhou, R. Sankar, X. Z. Xing, Z. X. Shi, Z. D. Han, B. Qian, J. H. Wang, Z. Zhu, J. L. Zhang, A. F. Bangura, N. E. Hussey, and X. Xu, Enhanced electron correlations in the binary stannide PdSn4: A homologue of the dirac nodal arc semimetal PtSn4, Phys. Rev. Mater. **1**, 064201 (2017).

[26] X. Z. Xing, C. Q. Xu, N. Zhou, B. Li, J. L. Zhang, Z. X. Shi, and X. Xu, Large linear magnetoresistance in a transition-metal stannide β-RhSn4, Appl. Phys. Lett. **109**, 122403 (2016).

[27] J. Xiong, S. K. Kushwaha, T. Liang, J. W. Krizan, M. Hirschberger, W. Wang, R. J. Cava, N. P. Ong, Evidence for the chiral anomaly in the dirac semimetal Na_3Bi, Science **350**, 413 (2015).

[28] T. Liang, Q. Gibson, M. N. Ali, M. Liu, R. J. Cava, and N. P. Ong, Ultrahigh mobility and giant magnetoresistance in the dirac semimetal Cd_3As_2, Nature Mater. **14**, 280 (2015).